Studies of the Mechanism of Selectivity of Protein Tyrosine Phosphatase 1B (PTP1B) Bidentate Inhibitors Using Molecular Dynamics Simulations and Free Energy Calculations

Lei Fang,[†] Huai Zhang,[‡] Wei Cui,[†] and Mingjun Ji*,[†]

College of Chemistry and Chemical Engineering, Graduate University of Chinese Academy of Sciences, P.O. Box 4588, Beijing 100049, PR China, and Laboratory of Computational Geodynamics, Graduate University of Chinese Academy of Sciences, Beijing 100049, PR China

Received March 26, 2008

Bidentate inhibitors of protein tyrosine phosphatase 1B (PTP1B) are considered as a group of ideal inhibitors with high binding potential and high selectivity in treating type II diabetes. In this paper, the binding models of five bidentate inhibitors to PTP1B, TCPTP, and SHP-2 were investigated and compared by using molecular dynamics (MD) simulations and free energy calculations. The binding free energies were computed using the Molecular Mechanics/Poisson−Boltzmann Surface Area (MM/PBSA) methodology. The calculation results show that the predicted free energies of the complexes are well consistent with the experimental data. The Molecular Mechanics/Generalized Born Surface Area (MM/GBSA) free energy decomposition analysis indicates that the residues ARG24, ARG254, and GLN262 in the second binding site of PTP1B are essential for the high selectivity of inhibitors. Furthermore, the residue PHE182 close to the active site is also important for the selectivity and the binding affinity of the inhibitors. According to our analysis, it can be concluded that in most cases the polarity of the portion of the inhibitor that binds to the second binding site of the protein is positive to the affinity of the inhibitors while negative to the selectivity of the inhibitors. We expect that the information we obtained here can help to develop potential PTP1B inhibitors with more promising specificity.

INTRODUCTION

Protein tyrosine phosphatase 1B (PTP1B), an intracellular nonreceptor protein tyrosine phosphatases (PTPs), is essential in the dephosphorylation of an insulin receptor in many cellular and biochemical studies.[1,2] Several independent experiments have demonstrated that the knockout of PTP1B in mice can result in insulin hypersensitivity, even in a high-fat diet.[3,4] Therefore, small molecular inhibitors of PTP1B are promising drug candidates for curing type II diabetes.

Due to high structure similarity across the PTPs family, it is challenging to find inhibitors specific to each PTP, such as PTP1B, TCPTP,[5] SHP-2,[6] LARC,[7] and CD45,[8] to avoid potential side effects.[9] In 1997, a second binding active site close to the conserved primary active site, also referred to as site B, was reported by Zhang and co-workers.[10] This binding site is not so conserved, and therefore it was believed that it should be exploited to design PTP1B inhibitors with good selectivity.

From then on, many bidentate compounds were found and proved to be potential and selective PTP1B inhibitors.[11−15] However, it is still very hard to improve the selectivity to a new level through the second binding site according to the experimental results.[11−15] In the current work, the binding models of five bidentate inhibitors (Figure 1) with PTP1B, TCPTP, and SHP-2 were predicted and analyzed by using molecular modeling techniques. The molecule dynamics (MD) simulation, free energy calculations, and free energy decomposition analysis were employed to investigate the detailed binding mechanisms of the bidentate inhibitors and

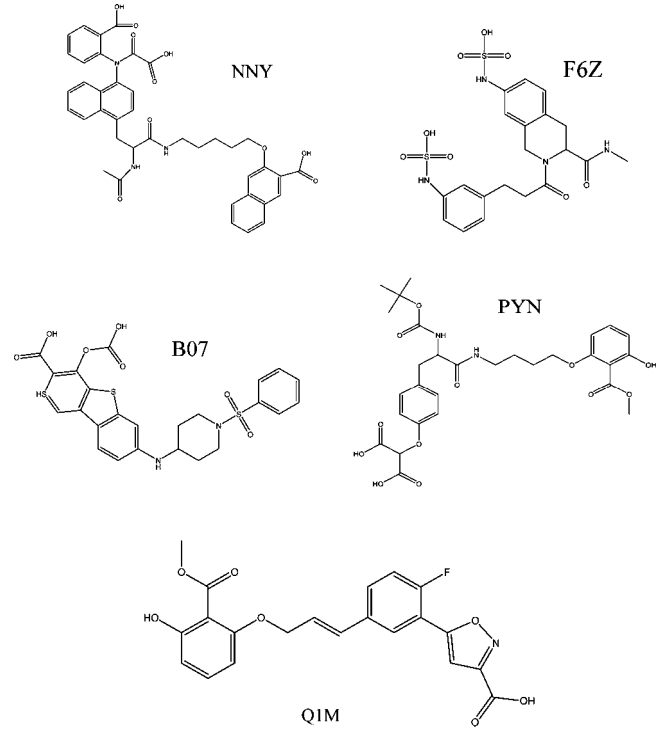

Figure 1. The 2-D structures of the bidentate inhibitors.

* Corresponding author phone: +8610 88256326; fax: +8610 88256093; e-mail: jmj@gucas.ac.cn.
[†] College of Chemistry and Chemical Engineering.
[‡] Laboratory of Computational Geodynamics.

10.1021/ci800104s CCC: $40.75
Published on Web 10/03/2008

to determine whether it is possible to design inhibitors with more promising selectivity based on the second binding site of PTP1B. Absolute binding free energies were calculated using the Molecular Mechanics/Possion-Boltzmann Surface Area (MM/PBSA) technique.[16−25] All inhibitors shown in Figure 1 were discovered in recent years and have the crystal structures complex with PTP1B.[11−15] They are about 1-fold to 30-fold more potential for PTP1B over TCPTP which shares about 80% homology with PTP1B.[26] Moreover, all of them have excellent selectivity for PTP1B over another protein PTP, SHP-2, which shares about 52% homology with PTP1B.

MATERIALS AND METHODS

1. The PTPs Structures. The starting structures for simulations, including the PTP1B complexes (PDB entries: 1NNY,[14] 2B07,[12] 2F6Z,[11] 1Q1M,[15] and 1PYN[13]), TCPTP (1L8k[26]), and SHP-2 (2SHP[26]), were downloaded from RCSB Brookhaven Protein Data Bank.[27]

The structure 2B07, which has a higher resolution (2.1 Å) than 2HNP (2.85 Å),[28] was selected to generate the *apo* PTP1B structure by deleting all the crystallographic water molecules and ligand in 2B07 using the SYBYL7.1 molecular simulation package.[29] The *apo* PTP1B structure was saved and named as 2B07M.

The structure of 2SHP is a dimer, so chain B was deleted. The missing side chains of some residues of 2SHP were added using the *tleap* program in AMBER9.[30] The missing hydrogen atoms were added by using *tleap* in AMBER9.[30] Then the *sander* program in AMBER9[30] was used to minimize the structure (the structure was immersed in the rectangular box of the TIP3P water molecules[31]) using the following steps: first, the water molecules were minimized by restraining the protein (5000 cycles of steepest descent and 5000 cycles of conjugate gradient minimizations); second, the side chains of the protein were minimized by restricting the backbone of the protein (5000 cycles of steepest descent and 5000 cycles of conjugate gradient minimizations); finally, the whole system was minimized without any restraint (5000 cycles of steepest descent and 5000 cycles of conjugate gradient minimizations). The water molecules were deleted using SYBYL7.1,[29] and the final structure of SHP-2 was saved and named as SHP-2M. The water molecules in 1L8K were deleted using SYBYL7.1,[29] and the final structure was saved and named as TCPTPM.

2. The Bidentate Inhibitors. The five bidentate inhibitors were extracted from the five PTP1B complexes (PDB entries: 1NNY, 2B07, 2F6Z, 1Q1M, and 1PYN). The missing hydrogen atoms of the inhibitors were added using SYBYL7.1.[29] The simplified codes of the complexes were used to represent the names of the inhibitors, which are NNY, B07, F6Z, Q1M, and PYN, respectively. The inhibitors were minimized using the Hartree−Fock(HF)/6−31G* optimization in Gaussian,[32] and atom partial charges were obtained by fitting the electrostatic potentials derived by Gaussian using the RESP fitting technique in AMBER9. The generations of the partial charges and the force field parameters for the inhibitors were accomplished using the *antechamber* program in AMBER9.[30]

3. The Protein/Inhibitor Complexes. Considering that these three proteins are homologous, rebuilding the binding models by using the molecular docking technique is obviously not the best choice. A simple and reliable strategy was used to construct the complexes−by aligning and merging−based on the assumption that the inhibitor has similar interaction modes with these three homologous proteins. The task was accomplished in SYBYL7.1.[29] Here the constructing process of the binding model of NNY with PTP1B is shown as an example to explain the strategy.

First, the 1NNY complex and 2B07M were structurally aligned, and then the ligand in 1NNY was extracted and merged into 2B07M. This new structure composed of the receptor (2B07M) and the ligand from the original complex (1NNY) was used as the starting structure for the following simulations. The reason for rebuilding the PTP1B complexes is to guarantee that the protein structures for all PTP1B complexes are the same. The same strategy was used to produce the other complexes.[33]

In the following molecular mechanics minimizations and MD simulations, the AMBER03 force field was used to establish the potentials of proteins,[34] and the general AMBER force field (gaff) was used to establish the potentials of inhibitors.[35] To neutralize the charge of the systems, counterions of Na^+ were placed on grids with the largest negative Coulombic potentials around the proteins, and then the whole system was immersed in the rectangular box of TIP3P water molecules.[31] The water box extended 12 Å away from any solute atoms.

4. Molecular Dynamics Simulations. Before the MD simulations, molecular mechanics optimizations were employed to relax the system using three steps: first, the water molecules were relaxed by restraining the protein (5000 cycles of steepest descent and 5000 cycles of conjugate gradient minimizations); second, the side chains of the protein were relaxed by restraining the backbone of the protein (5000 cycles of steepest descent and 5000 cycles of conjugate gradient minimizations); third, the whole system was relaxed without any restraint (5000 cycles of steepest descent and 5000 cycles of conjugate gradient minimizations). In MD simulations, Particle Mesh Ewald (PME) was employed to deal with the long-range electrostatic interactions.[36] The SHAKE procedure was employed to constrain all hydrogen atoms,[37] and the time step was set to 2.0 fs.

The system was gradually heated in the NVT ensemble from 0 to 310 K over 60 ps. Then, 1.4 ns MD simulations were performed under normal temperature (310 K). During the sampling process, coordinates were saved every 1 ps.

5. MM/PBSA Calculations. The binding free energy for each system was calculated using the MM/PBSA technique[24,25] according to

$$\Delta G_{binding} = G_{complex} - G_{protein} - G_{ligand} = \Delta E_{MM} + \Delta G_{PB} + \Delta G_{SA} - T\Delta S \quad (1)$$

where ΔE_{MM} is the molecular mechanics interaction energy between the protein and the inhibitor; ΔG_{PB} and ΔG_{SA} are the electrostatic and nonpolar contributions to desolvation upon inhibitor binding, respectively; and $-T\Delta S$ is the conformational entropy change, which was not considered because of the high computational cost and low prediction accuracy.[24]

Here, the polar part of desolvation was calculated by solving the Poisson−Boltzmann (PB) equations.[38] The grid size used to solve the Poisson−Boltzmann equation was 0.5

Å, and the values of interior dielectric constant and exterior dielectric constant were set to 1 and 80, respectively. ΔG_{SA} was estimated from the surface area. The protein−ligand binding free energy was calculated from the 120 snapshots taken from 0.2 to 1.4 ns MD simulation trajectories of the complex. The calculations for binding free energies were accomplished by using the *mm_pbsa* program in AMBER9.[30]

6. Inhibitor-Residue Free Energy Decomposition Analysis. Due to the high computational demand of the PB calculations, the interaction between each inhibitor and each protein residue was computed using the MM/GBSA decomposition process applied in the *mm_pbsa* program in AMBER9.[39] The binding interaction of each inhibitor-residue pair includes three terms: van der Waals contribution (ΔE_{vdw}), electrostatic contribution (ΔE_{ele}), and solvation contribution ($\Delta G_{\mathrm{GB}}+\Delta G_{\mathrm{SA}}$), where ΔE_{vdw} and ΔE_{ele} are nonbonded van der Waal interaction and electrostatic interaction between the inhibitor and each protein residue, which can be computed using the *sander* program in AMBER9.[30]

$$\Delta G_{inhibitor-residue} = \Delta E_{vdw} + \Delta E_{ele} + \Delta G_{GB} + \Delta G_{SA} \quad (2)$$

The polar contribution (ΔG_{GB}) of desolvation was computed using the generalized Born (GB) model, and the nonpolar contribution of desolvation (ΔG_{SA}) was computed using the surface area. The charges used in GB calculations were taken from the AMBER parameter set. All energy components were calculated using 120 snapshots from 0.2 ns to 1.4 ns.

RESULTS AND DISCUSSION

1. Stability and Flexibility of the Complexes. To explore the dynamic stability of these fifteen protein/inhibitor complexes and to ensure the rationality of the sampling strategy, root-mean-square displacement (rmsd) values of the protein backbone atoms during the production phase based on the starting snapshots were calculated and plotted in Figure 2.

The rmsd plots indicate that the conformations of the complexes usually achieve equilibrium at ∼200 ps, while to some conformations, this equilibrium time is ∼400 ps. As shown in Figure 2, the rank of the rmsd fluctuations for the complexes is SHP-2 > TCPTP > PTP1B, which is directly proportional to the experimental binding affinities of the inhibitors or the predicted binding free energies (see data in Table 1).

More detailed analysis of root-mean-square fluctuation (RMSF) versus the residue number for the fifteen protein/inhibitor complexes is illustrated in Figure 3. Overall, the structures with the same proteins share similar RMSF distributions and similar trends of dynamic features. To the PTP1B complexes, regions around the active site and site B (especially ARG24 and ARG254) show a rigid behavior. To the TCPTP complexes, regions around the active site and site B (especially ARG22 and ARG248) also show a rigid behavior, but the fluctuations are obviously larger than those of the PTP1B complexes. To the SHP-2 complexes, the fluctuations of the regions around the active site and site B (especially ARG18 and ARG251) are very significant, which is in good agreement with the relatively weak experimental binding affinity between the studied inhibitors and SHP-2.

2. Binding Free Energies Predicted by MM/PBSA. In MM/PBSA calculations, the affinity of a ligand binding to a protein can be estimated by the snapshots from a trajectory of the complex (single-trajectory protocol).[20] We first evaluated the performance of the MM/PBSA method on calculating the binding free energies of the inhibitors with the three PTP proteins. The binding free energies and the energy components of the complexes are shown in Table 1. It is encouraging that the predictions are well consistent with the experimental data ($\log K_{\mathrm{i}}$) (the correlation coefficient r and standard deviation SD are 0.88 and 8.4, respectively). It should be noted that in Table 1, four complexes do not have accurate experimental data: NNY/B07 (>500), F6Z/SHP-2 (>500), PYN/SHP-2 (>30), and Q1M/SHP-2 (no binding). For these four systems, 500, 500, 30, and 1000 were used as rough estimations for K_{i} in the correlation analysis. If these four systems are not considered, the correlation efficient r is 0.87.

To investigate which energy term determines the binding affinities of the inhibitors, we compared the correlations between the measured $\log K_{\mathrm{i}}$ and each of the four free energy components, ΔE_{ele}, ΔE_{vdw}, ΔG_{PB}, and ΔG_{SA}. If we did not consider four systems without quantitative experimental data, the correlation coefficients are 0.72 for ΔE_{ele}, 0.56 for ΔE_{vdw}, −0.68 for ΔG_{PB}, and 0.52 for ΔG_{SA}, respectively, suggesting that the polar contribution (electrostatic interaction and the polar part of desolvation) dominates the binding of inhibitors. We then analyzed the nonpolar ($\Delta E_{\mathrm{vdw}}+\Delta G_{\mathrm{SA}}$) and the electrostatic contributions ($\Delta E_{\mathrm{ele}}+\Delta G_{\mathrm{PB}}$) to the binding free energies. The electrostatic contribution achieves better correlation ($r = 0.80$) with the nonpolar contribution ($r = 0.58$). Therefore, it seems that the electrostatic contributions are more important than the nonpolar contributions to the inhibitor binding.

3. Mechanisms of Binding and Selectivity for Inhibitors. In order to get the contribution of each peptide residue to the total binding energy, free energy decomposition was employed.[39−41] According to the experimental data (Table 1), the inhibitors can be divided into two categories: inhibitors of high selectivity (Q1M and PYN) and inhibitors of low selectivity (NNY, B07, and F6Z). Overall, when the inhibitors belong to the same category (high or low selectivity), the interaction spectrums between the inhibitors and the same enzyme are quite similar. In the following discussions, the comparison between PTP1B and TCPTP is the keystone of the study. Moreover, the comparison of PTP1B and SHP-2 was also discussed. In order to understand the role of site B, the interactions between the inhibitors and the residues in site B were discussed.

3.1. The Analysis of Binding and Selectivity for Inhibitor NNY. Inhibitor NNY is a bidentate inhibitor reported by Szczepankiewicz et al.,[14] which shows modest selectivity for PTP1B over TCPTP but excellent selectivity over SHP-2, and the corresponding selectivity ratios are 2 and 104, respectively. Unfortunately, Szczepankiewicz and co-workers did not report the crystal structure of the TCPTP complexes and the SHP-2 complexes,[14] so the binding models of the TCPTP/NNY and the SHP-2/NNY complexes were rebuilt to investigate the mechanisms of the selectivity.

The predicted binding free energies of NNY with PTP1B, TCPTP, and SHP-2 are −99.23, −87.87, and −80.83 kcal/mol, respectively. This predicted binding rank is consistent

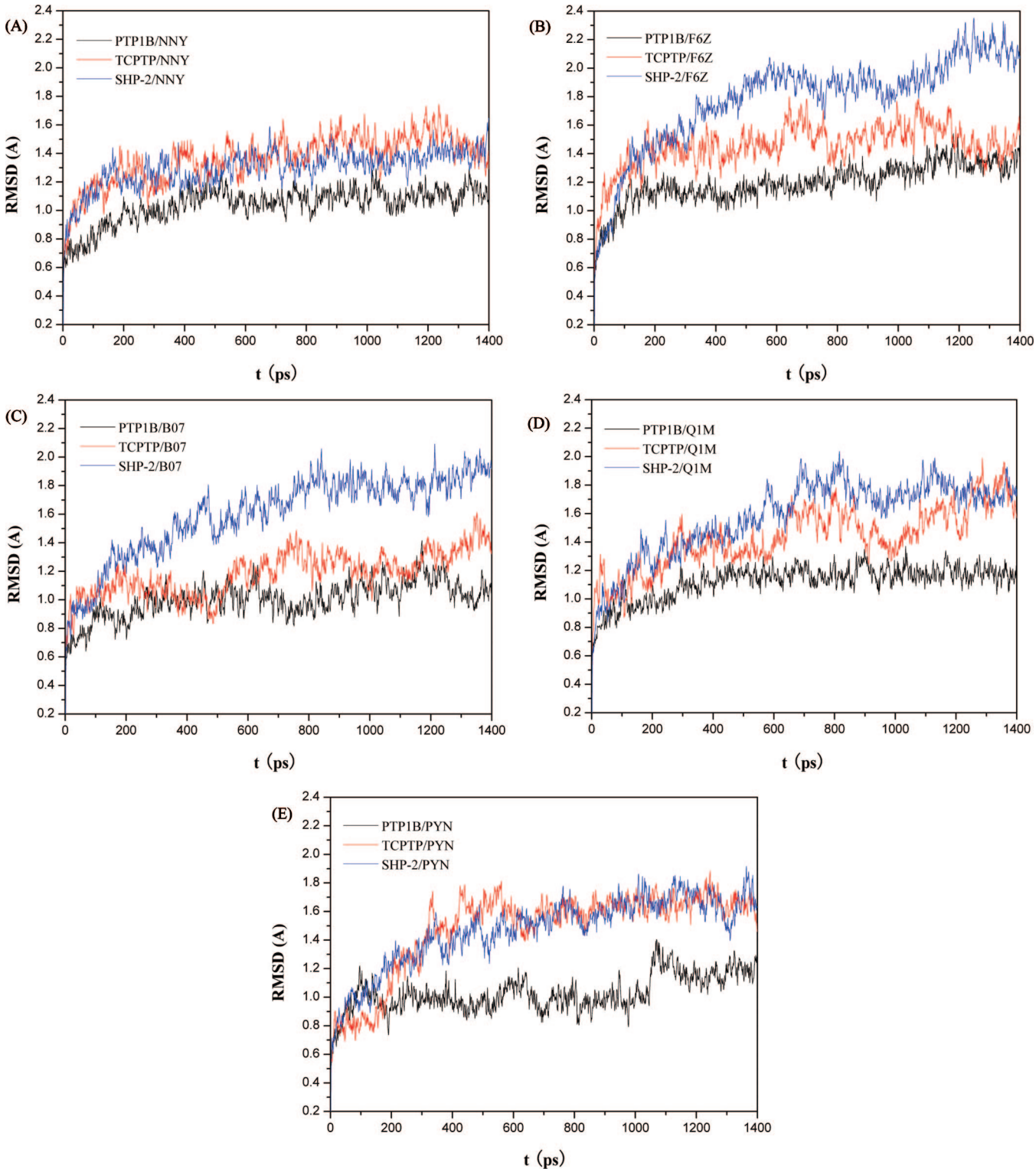

Figure 2. Root-mean-square displacements (rmsd) of the backbone atoms (CA, N, C) of the complexes with respect to the first snapshot as a function of time for (A) NNY, (B)F6Z, (C) B07, (D) Q1M, and (E) PYN.

with the experimental results. According to the predicted binding models of the complexes shown in Figure 4 the inhibitor NNY binds to both the active site and site B of the proteins, except SHP-2. The inhibitor did not bind so well with site B of SHP-2. These three schematic representations of interaction give us a direct view about the selectivity of NNY.

The primary active site of PTP1B includes seven residues from CYS215 to ARG221 (CYS212 to ARG218 in TCPTP and SHP2). The residues close to the active sites are TYR46, LYS120, and PHE182 in PTP1B (TYR44 and LYS109 in TCPTP, TYR32, ARG115, and LYS119 in SHP-2). The residues composed of site B of PTP1B include MET258, GLY259, GLN262, and GLN266, and two key arginine residues: ARG24 and ARG254.

The NNY/residue interaction spectrums calculated by the MM/GBSA energy decomposition analysis are shown in Figure 5. The crucial residues are mainly located in or close

Table 1. Free Energy Result and Energy Components Contributing to the Binding Free Energy (kcal/mol)

ligand-protein complex	ΔE_{ele}	ΔE_{vdw}	ΔG_{SA}	ΔG_{PB}	ΔG_{total} (pred) [a]	K_i (exp)
NNY - PTP1B	−417.53	−57.96	−8.75	385.55	−99.23	0.022
NNY - TCPTP	−426.60	−54.12	−8.78	401.64	−87.87	0.049
NNY - SHP-2	−435.97	−64.86	−9.33	429.33	−80.83	2.49
B07 - PTP1B	−284.66	−37.31	−5.55	259.39	−68.14	0.37
B07 - TCPTP	−303.02	−40.77	−6.52	283.55	−66.76	0.39
B07 - SHP−2	−358.03	−31.45	−5.18	337.16	−57.49	>500
F6Z - PTP1B	−221.75	−45.87	−5.77	204.60	−68.79	4.8[b]
F6Z - TCPTP	−222.84	−41.35	−5.86	204.49	−65.56	9.9[b]
F6Z - SHP−2	−248.25	−39.49	−5.62	246.13	−47.22	>500[b]
PYN - PTP1B	−287.89	−51.29	−7.49	279.00	−67.67	3.2
PYN - TCPTP	−318.21	−38.79	−6.67	303.57	−60.10	24.6
PYN - SHP-2	−349.30	−33.97	−5.82	338.79	−50.30	−30
Q1M - PTP1B	−172.64	−41.19	−5.63	168.91	−50.56	6.9
Q1M - TCPTP	−154.72	−31.46	−5.03	150.05	−41.16	164
Q1M - SHP-2	−166.26	−31.15	−4.68	162.62	−39.47	N/A

[a] The predictions do not include the contribution of conformational entropy. [b] IC_{50}.

to the active site and in site B of the proteins (such as ARG221 in PTP1B, ARG218 in TCPTP and SHP-2 are located in the active site, LYS120, PHE182 in PTP1B, ASN109 in TCPTP, and ARG115 in SHP2 are close to the active site, ARG24 and ARG254 in PTP1B, ARG22 and ARG248 in TCPTP, ARG251 in SHP-2 are located in site B). For all three complexes, the inhibitor NNY and the residues in the active site show strong interaction. Here, the energy contributions for the residues composed of the active site (CYS215 to ARG221 in PTP1B, CYS212 to ARG218 in TCPTP, CYS212 to ARG218 in SHP-2) are summed and are −34.36, −34.56, and −34.72 kcal/mol, respectively. Therefore, the residues in the active site of the three PTP proteins give similar contribution for the NNY binding. This is reasonable because the active sites of the three proteins have similar residues and volume. The schematic diagrams in Figure S1 in the Supporting Information also show the similarity. Hydrogen bonds were formed between the residues in the active site and the carboxyl and carbonyl of the ligands. The hydrophobic interaction was formed between the residues in the active site and the aromatic rings in the ligands. Some residues near the active site are also involved in the hydrogen bonds and hydrophobic interaction, such as TYR46, LYS120, and PHE182 in PTP1B.

When considering the contribution of site B, significant difference is not found between PTP1B and TCPTP but is found between PTP1B and SHP-2. To PTP1B and TCPTP, the two essential arginine residues in site B (ARG24 and ARG254 in PTP1B, ARG22, and ARG248 in TCPTP) have similar interactions with NNY (−8.33 and −6.41 kcal/mol for PTP1B, −8.10 and −6.45 kcal/mol for TCPTP) (Figure 5). As shown by the schematic diagrams in Figure S1 in the Supporting Information, an important residue in site B of PTP1B, GLN262 forms a hydrogen bond with NNY. But GLN256 in TCPTP does not form any hydrogen bond with the ligands.

Compared with that between NNY and PTP1B, the interaction between NNY and the essential arginine residues (ARG18 and ARG 251) of site B in SHP-2 are much weaker (−0.47 and −4.65 kcal/mol, respectively) (Figure 5), and no hydrogen bond is formed with the ligands. We believe that this is a very important reason to explain the high selectivity between PTP1B and SHP-2.

According to the free energy decomposition analysis, the inhibitor NNY shows its advantage of selectivity based on site B over SHP-2, but it still does not escape from the high homology between PTP1B and TCPTP. According to the analysis result, the residues LYS 120, PHE182, and GLN262 are helpful to improve the selectivity. High polarity and large volume may be not helpful to improve the selectivity considering the high polarity of the two binding sites.

3.2. The Analysis of Binding and Selectivity for Inhibitor F6Z. Inhibitor 2F6Z is another bidentate inhibitor reported by Klopfenstein in 2006.[11] According to the experimental date, this inhibitor shows modest selectivity for PTP1B over TCPTP (the ratio is about 2) and excellent selectivity over SHP-2 (the IC_{50} of SHP-2 is larger than 500).

The binding free energies of F6Z with PTP1B, TCPTP, and SHP-2 are −68.79, −65.56, and −47.22 kcal/mol, respectively. The difference of the binding energy between PTP1B complexes and TCPTP complexes is small, which is consistent with the experiment. The predicted free energy between F6Z and SHP-3 is much weaker than those between F6Z and other two proteins.

As shown in Figure 6, the inhibitor/residue interaction profiles of PTP1B and TCPTP are quite similar. The total contributions of the active site residues for inhibitor binding are −33.34, −31.90, and −27.23 kcal/mol, respectively. Quite different from the inhibitor NNY, the contributions of the active site residues for the three PTP proteins are different because the portion of F6Z that binds to the active site has the lower polarity and small volume compared with NNY. The binding characteristics of F6Z are quite similar to that of NNY (see Figure S2 in the Supporting Information): (1) hydrogen bonds could be found between the residues in the active site and the sulfuric acid groups of these two inhibitors; (2) the hydrophobic interactions were formed between the residues in the active site and the aromatic rings of the inhibitors; and (3) some residues near the active site are also involved in the hydrophobic interaction, such as PHE182 in PTP1B.

To PTP1B and TCPTP, the two essential arginine residues in site B (ARG24 and ARG254 in PTP1B, and ARG22 and ARG248 in TCPTP) form similar interactions with F6Z (−4.52 and −6.53 kcal/mol for PTP1B, and −4.72 and −6.75 kcal/mol for TCPTP). As shown by Figure S2 in the Supporting Information, F6Z forms hydrogen bonds with the two essential arginine residues of both PTP1B and TCPTP. The free energy difference between the PTP1B complexes and the TCPTP complexes is mainly related to GLN262 (Figure 6A).

Compared with NNY, by decreasing the polarity and volume at the portion that binds to the active site, the inhibitor shows different interaction capabilities with the residues in the active site. But little improvement over TCPTP is observed at site B. Moreover, because of the decrease of the polarity in both parts that binds to the active site and site B, the binding affinity decreases obviously. However, it really shows the improvement of selectivity for SHP-2. But whether in the active site or in site B, the binding of the inhibitor becomes weaker compared with that of NNY.

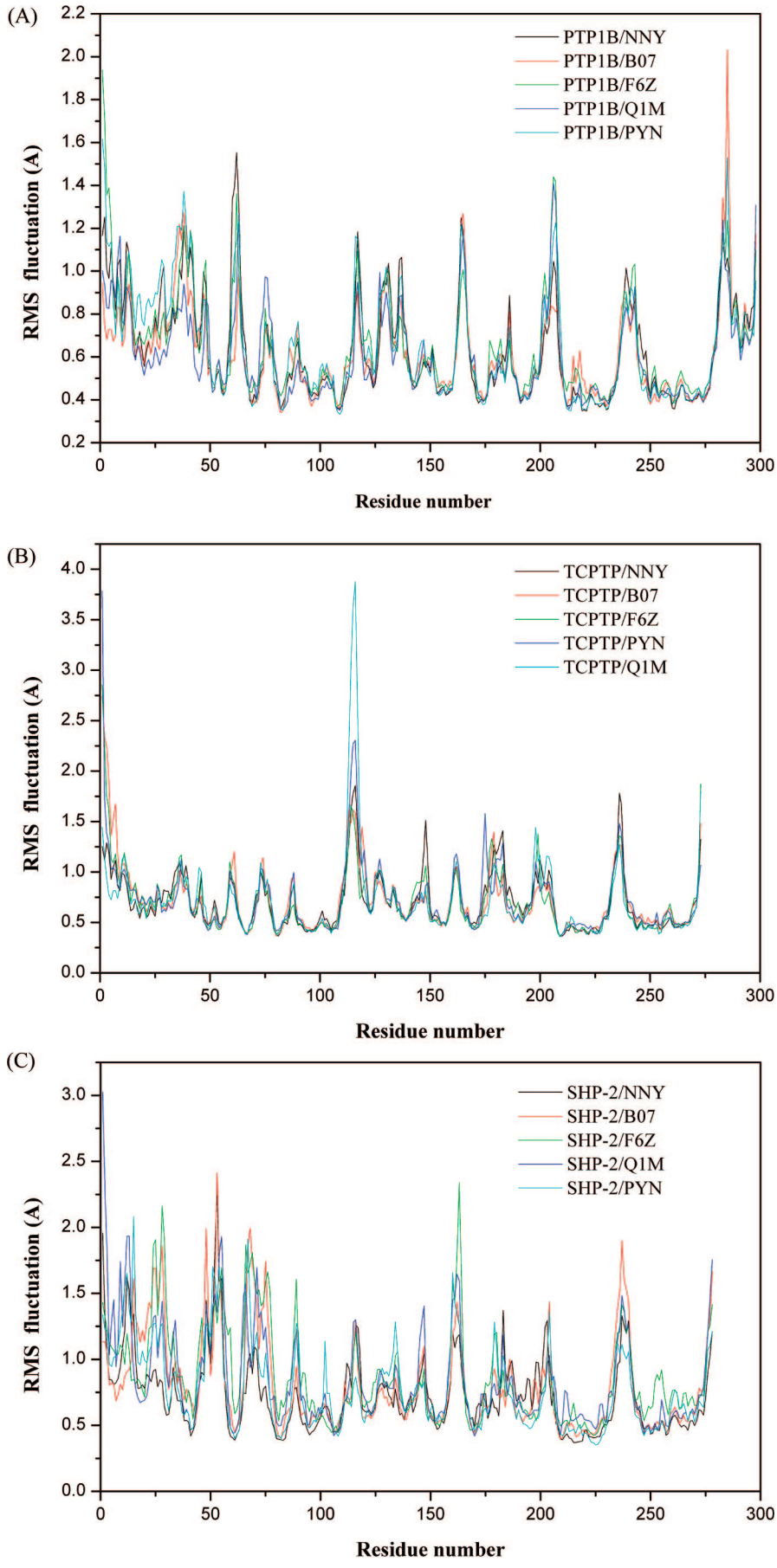

Figure 3. Root-mean-square fluctuation (RMSF) of the backbone atoms (CA, N, C) versus residue number for (A) the PTP1B complex, (B) the TCPTP complex, and (C) the SHP-2 complex.

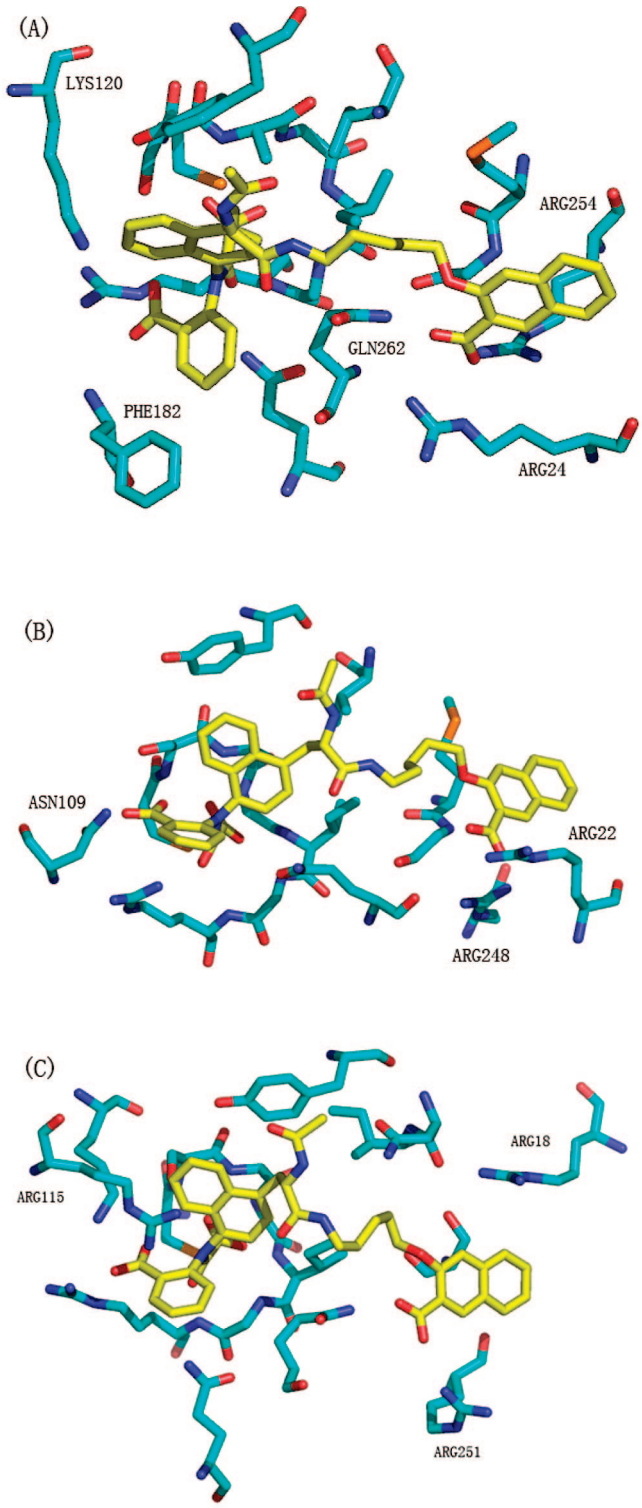

Figure 4. Inhibitor-protein interaction diagrams of (A) the PTP1B/NNY complex, (B) the TCPTP/NNY complex, and (C) the SHP-2/NNY complex.

3.3. The Analysis of Binding and Selectivity for Inhibitor B07. Inhibitor B07 is an inhibitor of PTP1B reported by Lee et al.[12] It is similar to the above two inhibitors, but it has its own characteristics. Similar to F6Z, B07 has good selectivity of PTP1B over SHP-2, but it does not show obvious selectivity over TCPTP.

The predicted binding free energies of B07 with PTP1B, TCPTP, and SHP-2 are −68.14,−66.76 and −57.49 kcal/mol, respectively, which is consistent with the experiments.[12]

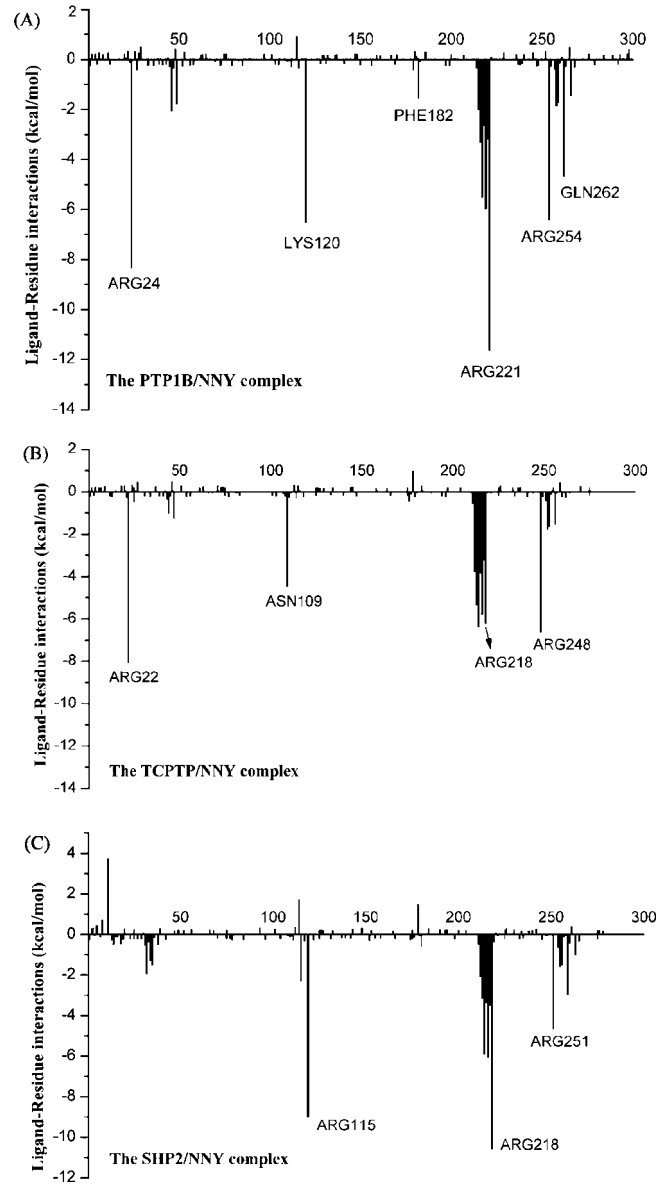

Figure 5. Inhibitor-residue interaction spectrums of (A) the PTP1B/NNY complex, (B) the TCPTP/NNY complex, and (C) the SHP-2/NNY complex.

The schematic representation of interactions between B07 and SHP-2 is shown in Figure 7. According to the energy decomposition analysis shown in Figure 8, the inhibitor B07 mainly forms effective interaction with the active site residues of the three PTP proteins. The contributions of the active site residues for binding are −32.87, −34.97 and −25.65 kcal/mol, respectively. Similar to NNY and F6Z, the interaction between B07 and SHP-2 is still very weak.

It seems that this bidentate inhibitor does not bind firmly with site B of PTP1B. The interaction between B07 and the two arginine residues is not so strong, because the part of B07 binding to site B was not so polar, the linker between the part binding to the active and the part binding to the site B was rigid and short. GLN262 in PTP1B was no longer an important residue here. Similar to the former results, the interaction between the inhibitor B07 and site B of SHP-2 is still very weak.

B07 is also not a successful bidentate inhibitor. Decreasing its polarity (from carboxylic acid to sulfonamide) does not help to improve the selectivity of PTP1B over

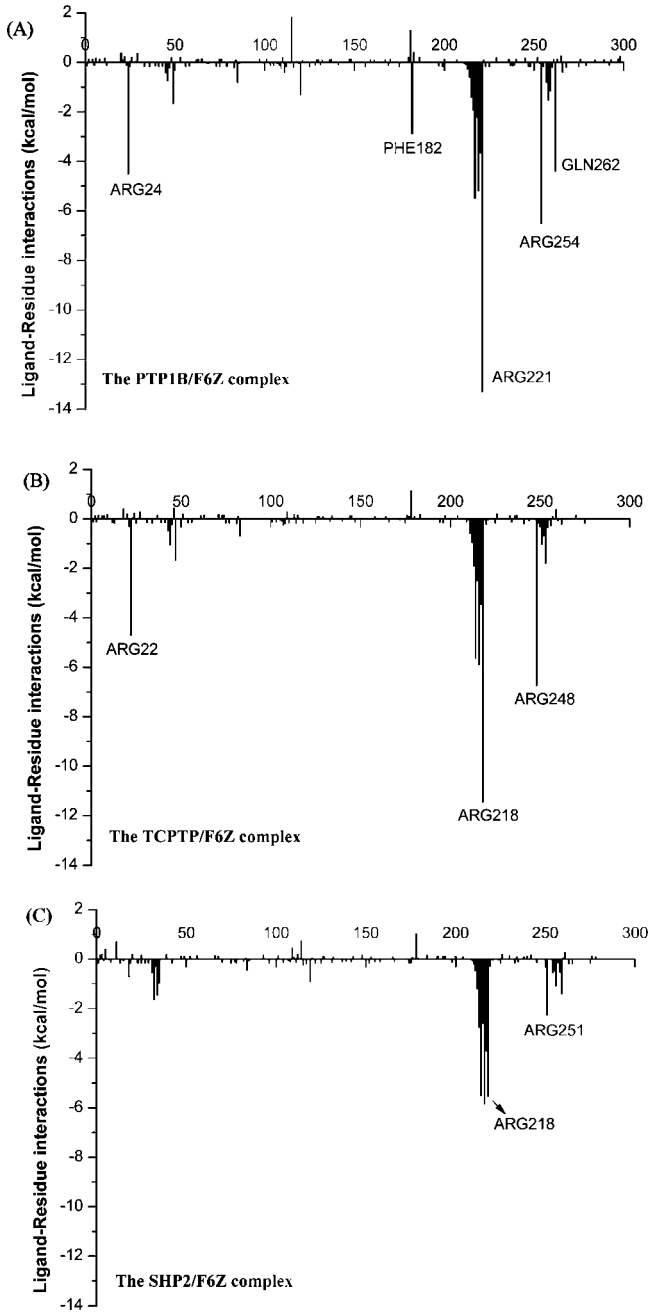

Figure 6. Inhibitor-residue interaction spectrums of (A) the PTP1B/F6Z complex, (B) the TCPTP/F6Z complex, and (C) the SHP-2/F6Z complex.

TCPTP. Like NNY and F6Z, B07 is very selective for PTP1B over SHP-2.

3.4. The Analysis of Binding and Selectivity for Inhibitor Q1M. Q1M is an inhibitor discovered in 2003 by Liu et al.[15] It is a moderately potent and highly selective PTP1B inhibitor. It does not show inhibitory activity against SHP-2 even at the highest concentration tested, and PTP1B is about 30-fold more potent than TCPTP.

The predicted binding free energies of Q1M with PTP1B, TCPTP, and SHP-2 are −50.56, −41.16, and −39.47 kcal/mol, respectively. The binding of TCPTP with Q1M is weaker than that of PTP1B with Q1M, which is consistent with the experimental result. The binding of SHP-2 with Q1M is even weaker than that of TCPTP with Q1M, suggesting that Q1M does not show effective inhibitory activity against SHP-2.

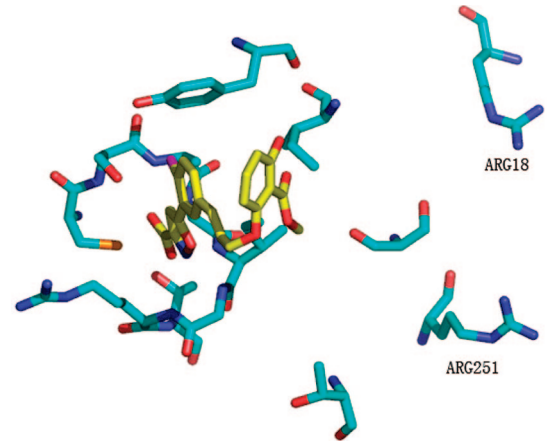

Figure 7. Inhibitor-protein interaction diagram of SHP-2 with B07.

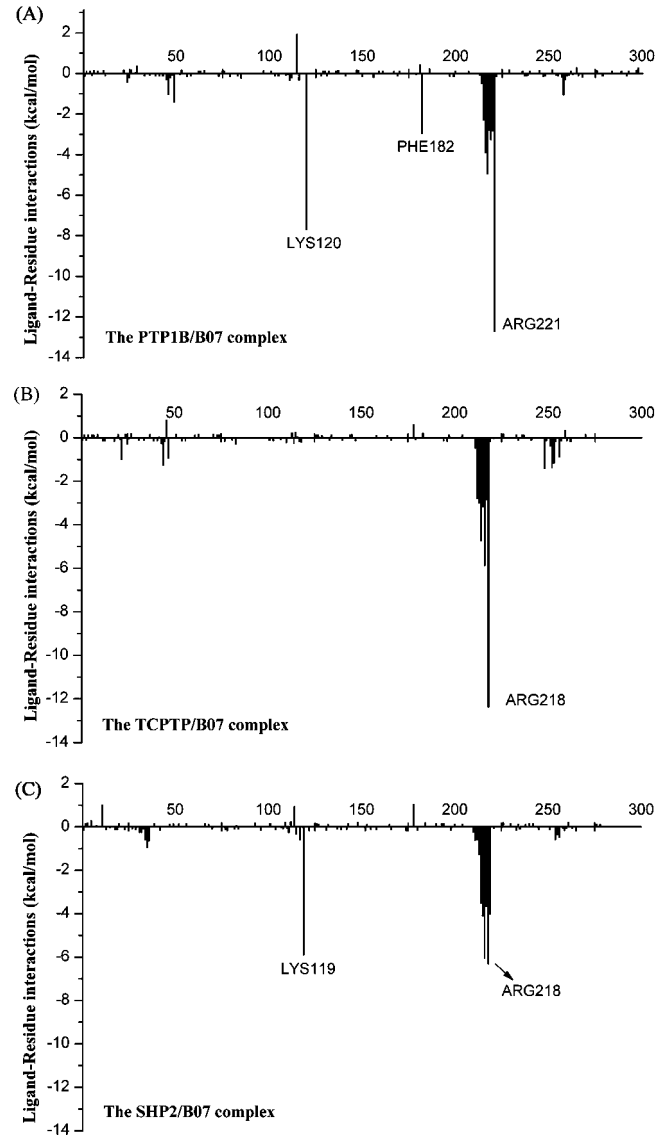

Figure 8. Inhibitor-residue interaction spectrums of (A) the PTP1B/B07 complex, (B) the TCPTP/B07 complex, and (C) the SHP-2/B07 complex.

The binding models of the inhibitor with the PTP proteins are shown in Figure 9. According to the figures, it is observed that the inhibitor binds to both the active site and site B of PTP1B, while it mainly binds into the primary active sites

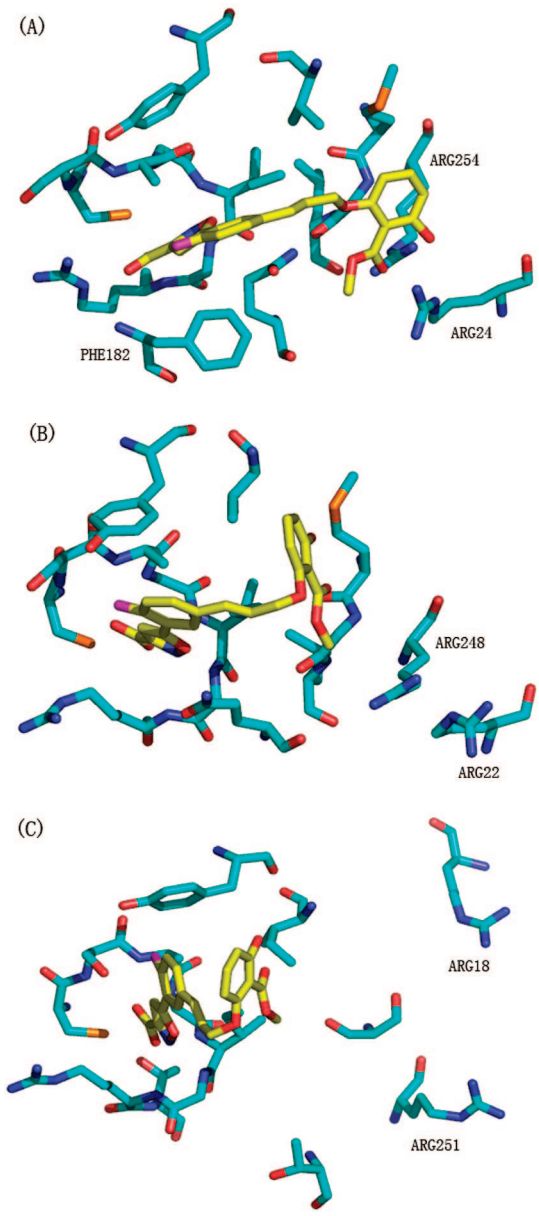

Figure 9. Inhibitor-protein interaction diagrams of (A) the PTP1B/Q1M complex, (B) the TCPTP/Q1M complex, and (C) the SHP-2/Q1M complex.

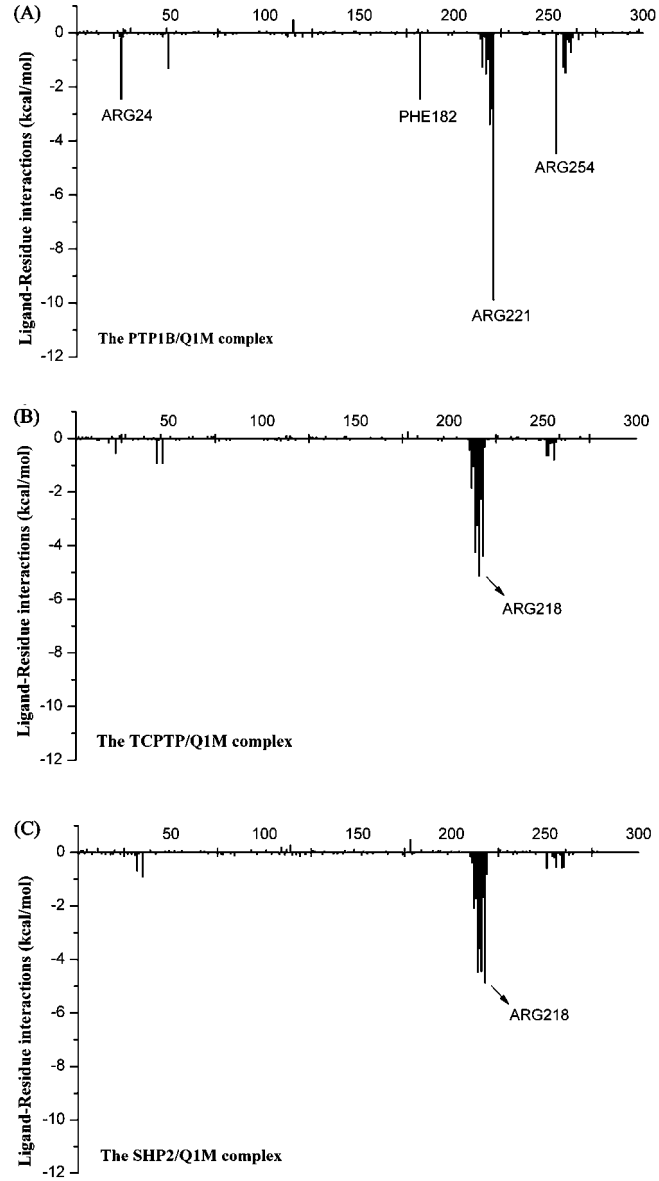

Figure 10. Inhibitor-residue interaction spectrums of (A) the PTP1B/Q1M complex, (B) the TCPTP/Q1M complex, and (C) the SHP-2/Q1M complex.

of TCPTP and SHP-2. As shown by Figure S4 in the Supporting Information, it can be found that hydrogen bonds were formed between the active site residues and the carboxyl of the ligand. The hydrophobic interaction was formed between the active site residues and the heterocycle group of the ligand. Some residues near the active site are also involved in the hydrogen bonds and hydrophobic interaction, such as PHE182 in PTP1B.

In site B, only ARG254 in PTP1B formed hydrogen bonds with the ligand. The ligand formed a strong hydrophobic interaction with PTP1B and a weak hydrophobic interaction with TCPTP. This is another evidence to explain why Q1M has high selectivity. It is also an evidence to show the advantage of site B, suggesting that site B is very important to improve the selectivity.

The detailed information of the free energy decomposition for Q1M is shown in Figure 10. Totally, for all three PTP proteins, the affinities of Q1M decrease compared with those of the above-discussed inhibitors with low selectivity. Either polarity or volume of Q1M is less than that of NNY. The decrease of the volume helps to improve the selectivity. Only molecules with the appropriate volume can fit into both of the sites of PTP1B, while they cannot for TCPTP and SHP-2.

3.5. The Analysis of Binding and Selectivity for Inhibitor PYN. PYN is an inhibitor of PTP1B discovered in 2003 by Pei et al.[13] This inhibitor was potent and selective. It is 7.7-fold selective against TCPTP and more than 30-fold selective against SHP-2. PYN has similar polarity to the part that binds to the active sites as NNY, B07 and F6Z, but the polarity of the part that binds to site B is very low. This is quite similar to the inhibitor Q1M.

The binding free energies of PYN with PTP1B, TCPTP, and SHP-2 are −68.14, −66.76, and −57.49 kcal/mol, respectively. This rank is reasonable to explain the experimental result. The inhibitor/residue interaction spectrums are shown in Figure 11. The interactions between PYN and site B is not strong because the portion of PYN that binds to

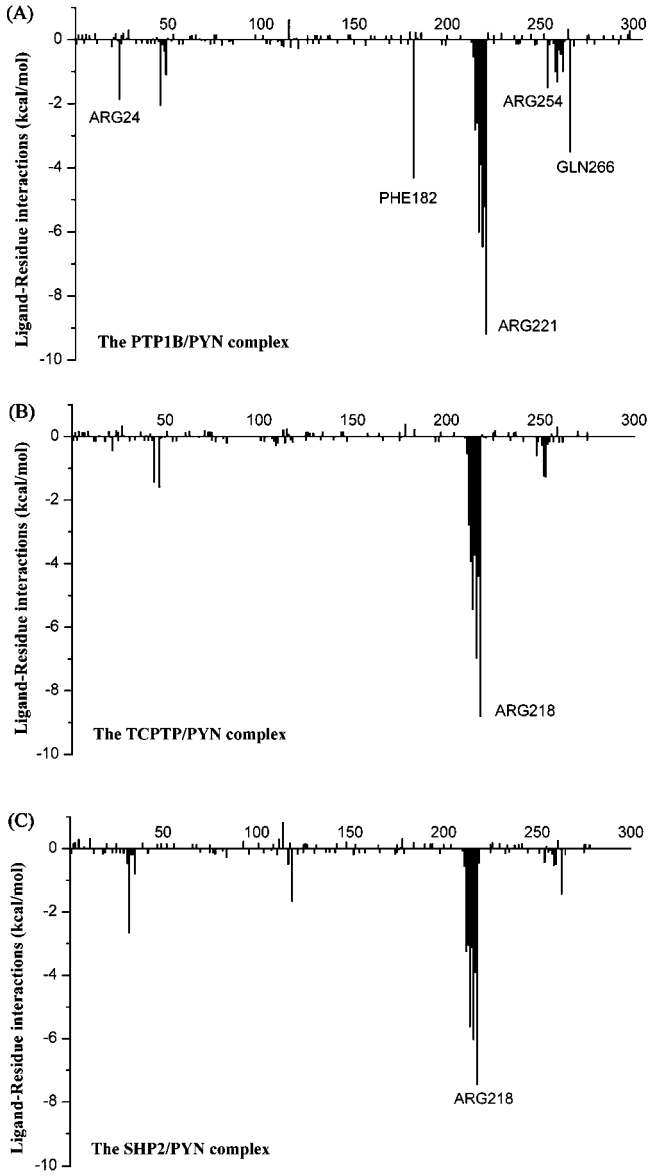

Figure 11. Inhibitor-residue interaction spectrums of (A) the PTP1B/PYN complex, (B) the TCPTP/PYN complex, and (C) the SHP-2/PYN complex.

site B is not so polar. For the three proteins, the difference of the binding free energies of Q1M is mainly caused by the residues in site B and the residues close to the active site while not the residues in the active sites. The interactions between the two important arginine residues in site B and PYN are −1.88, −0.46, and −0.19 kcal/mol for ARG24, respectively, and −1.52,−0.61, and −0.45 kcal/mol for ARG254, respectively. The difference is very important to improve the selectivity of PYN. GLN262 is also an important player for selectivity. Similar to Q1M, PYN does not form an important interaction with site B of SHP-2, as shown in Figure 12.

According to the analysis based on molecular modeling, it can be found that the bidentate inhabitation strategy is only useful to improve the selectivity of PTP1B over SHP-2. The inhibitors with good selectivity are those candidates when they can succeed in escaping from the highly identical sequence of PTP1B and TCPTP, though they lose some binding affinities.

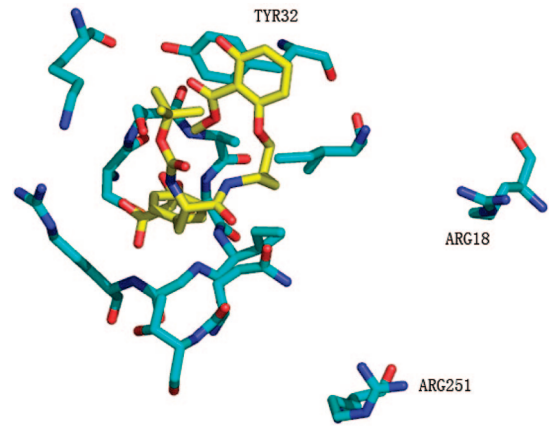

Figure 12. Inhibitor-protein interaction diagram of the SHP-2/ PYN complex.

CONCLUSION

In this study, fifteen complexes of five bidentate inhibitors and three proteins were built based on the simple aligning and merging strategy. According to the MD simulations, MM/PBSA free energy calculations, and MM/GBSA free energy decomposition analyses, we can make the following conclusions.

To inhibitors that are not so selective, like NNY, they have strong interactions with the arginine residues in site B of the three PTP proteins. But to inhibitors that are more selective, like Q1M, they only form effective interactions with the arginine residues in site B of PTP1B. This proved that the second binding site is very important for designing inhibitors with good selectivity over low homology protein like SHP-2. To TCPTP, the improvement depends on the inhibitor itself: some inhibitors can use the advantage of the second binding site, some cannot. To most of the inhibitors (four-fifths in this paper, except B07), the polarity of the part that binds to site B of the protein is positive to the potential of the inhibitor and negative to the selectivity of the inhibitor.

In summary, to design an ideal bidentate inhibitor of PTP1B, one thing is to control the polarity and volume of the portion that binds to the active site. Reasonable design can help to maintain the potential and improve the selectivity, like F6Z. The other important thing is to design the molecule with a proper length which helps to form interaction with only site B of PTP1B, like Q1M. Also, improving the interaction between the inhibitor and LYS120 and PHE182 around the active site and GLN262 in site B may be a good strategy to improve the selectivity of the bidentate inhibitors. So an ideal bidentate ligand should have aromatic rings or a heterocycle, some hydrogen donors and receptors, and a flexible linker, but, however, finding an ideal inhibitor of PTP1B by using site B does not seem like a very ideal method.

ACKNOWLEDGMENT

The project was supported by the Natural Science Foundation of China (No. 20373089) and the Start-up Foundation of the Graduate University of Chinese Academy of Sciences (No. M3004). We thank Prof. Xiaojie Xu in the Department of Chemistry of Peking University for providing access to computer software such as AMBER.

Supporting Information Available: Figures S1−S4. This material is available free of charge via the Internet at http://pubs.acs.org.

REFERENCES AND NOTES

(1) Byon, J. C. H.; Kusari, A. B.; Kusari, J. Protein-tyrosine phosphatase-1B acts as a negative regulator of insulin signal transduction. *Mol. Cell. Biochem.* **1998**, *182*, 101–108.

(2) Tonks, N. K.; Diltz, C. D.; Fischer, E. H. Purification of the Major Protein-Tyrosine-Phosphatases of Human-Placenta. *J. Biol. Chem.* **1988**, *263*, 6722–6730.

(3) Klaman, L. D.; Boss, O.; Peroni, O. D.; Kim, J. K.; Martino, J. L.; Zabolotny, J. M.; Moghal, N.; Lubkin, M.; Kim, Y. B.; Sharpe, A. H.; tricker-Krongrad, A.; Shulman, G. I.; Neel, B. G.; Kahn, B. B. Increased energy expenditure, decreased adiposity, and tissue-specific insulin sensitivity in protein-tyrosine phosphatase 1B-deficient mice. *Mol. Cell. Biol.* **2000**, *20*, 5479–5489.

(4) Elchebly, M.; Payette, P.; Michaliszyn, E.; Cromlish, W.; Collins, S.; Loy, A. L.; Normandin, D.; Cheng, A.; Himms-Hagen, J.; Chan, C. C.; Ramachandran, C.; Gresser, M. J.; Tremblay, M. L.; Kennedy, B. P. Increased insulin sensitivity and obesity resistance in mice lacking the protein tyrosine phosphatase-1B gene. *Science* **1999**, *283*, 1544–1548.

(5) Tiganis, T.; Kemp, B. E.; Tonks, N. K. The protein-tyrosine phosphatase TCPTP regulates epidermal growth factor receptor-mediated and phosphatidylinositol 3-kinase-dependent signaling. *J. Biol. Chem.* **1999**, *274*, 27768–27775.

(6) Hof, P.; Pluskey, S.; Dhe-Paganon, S.; Eck, M. J.; Shoelson, S. E. Crystal structure of the tyrosine phosphatase SHP-2. *Cell* **1998**, *92*, 441–450.

(7) Cheng, A.; Dube, N.; Gu, F.; Tremblay, M. L. Coordinated action of protein tyrosine phosphatases in insulin signal transduction. *Eur. J. Biochem.* **2002**, *269*, 1050–1059.

(8) Penninger, J. M.; Irie-Sasaki, J.; Sasaki, T.; Oliveira-dos-Santos, A. J. CD45: new jobs for an old acquaintance. *Nat. Immunol.* **2001**, *2*, 389–396.

(9) YouTen, K. E.; Muise, E. S.; Itie, A.; Michaliszyn, E.; Wagner, J.; Jothy, S.; Lapp, W. S.; Tremblay, M. L. Impaired bone marrow microenvironment and immune function in T cell protein tyrosine phosphatase-deficient mice. *J. Exp. Med.* **1997**, *186*, 683–693.

(10) Puius, Y. A.; Zhao, Y.; Sullivan, M.; Lawrence, D. S.; Almo, S. C.; Zhang, Z. Y. Identification of a second aryl phosphate-binding site in protein-tyrosine phosphatase 1B: A paradigm for inhibitor design. *Proc. Natl. Acad. Sci. U.S.A.* **1997**, *94*, 13420–13425.

(11) Klopfenstein, S. R.; Evdokimov, A. G.; Colson, A. O.; Fairweather, N. T.; Neuman, J. J.; Maier, M. B.; Gray, J. L.; Gerwe, G. S.; Stake, G. E.; Howard, B. W.; Farmer, J. A.; Pokross, M. E.; Downs, T. R.; Kasibhatla, B.; Peters, K. G. 1,2,3,4-tetrahydroisoquinolinyl sulfamic acids as phosphatase PTP1B inhibitors. *Bioorg. Med. Chem. Lett.* **2006**, *16*, 1574–1578.

(12) Moretto, A. F.; Kirincich, S. J.; Xu, W. X.; Smith, M. J.; Wan, Z. K.; Wilson, P.; Follows, B. C.; Binnun, E.; Joseph-McCarthy, D.; Foreman, K.; Erbe, D. V.; Zhang, Y. L.; Tam, S. K.; Tam, S. Y.; Lee, J. Bicyclic and tricyclic thiophenes as protein tyrosine phosphatase 1B inhibitors. *Bioorg. Med. Chem.* **2006**, *14*, 2162–2177.

(13) Moretto, A. F.; Kirincich, S. J.; Xu, W. X.; Smith, M. J.; Wan, Z. K.; Wilson, D. P.; Follows, B. C.; Binnun, E.; Joseph-McCarthy, D.; Foreman, K.; Erbe, D. V.; Zhang, Y. L.; Tam, S. K.; Tam, S. Y.; Lee, J. Discovery and SAR of novel, potent and selective protein tyrosine phosphatase 1B inhibitors. *Bioorg. Med. Chem. Lett.* **2003**, *13*, 3129–3132.

(14) Szczepankiewicz, B. G.; Liu, G.; Hajduk, P. J.; Abad-Zapatero, C.; Pei, Z.; Xin, Z. L.; Lubben, T. H.; Trevillyan, J. M.; Stashko, M. A.; Ballaron, S. J.; Liang, H.; Huang, F.; Hutchins, C. W.; Fesik, S. W.; Jirousek, M. R. Discovery of a potent, selective protein tyrosine phosphatase 1B inhibitor using a linked-fragment strategy. *J. Am. Chem. Soc.* **2003**, *125*, 4087–4096.

(15) Liu, G.; Xin, Z. L.; Pei, Z. G.; Hajduk, P. J.; Abad-Zapatero, C.; Hutchins, C. W.; Zhao, H. Y.; Lubben, T. H.; Ballaron, S. J.; Haasch, D. L.; Kaszubska, W.; Rondinone, C. M.; Trevillyan, J. M.; Jirousek, M. R. Fragment screening and assembly: A highly efficient approach to a selective and cell active protein tyrosine phosphatase 1B inhibitor. *J. Med. Chem.* **2003**, *46*, 4232–4235.

(16) Wang, W.; Kollman, P. A. Free energy calculations on dimer stability of the HIV protease using molecular dynamics and a continuum solvent model. *J. Mol. Biol.* **2000**, *303*, 567–582.

(17) Hou, T. J.; Guo, S. L.; Xu, X. J. Predictions of binding of a diverse set of ligands to gelatinase-A by a combination of molecular dynamics and continuum solvent models. *J. Phys. Chem. B* **2002**, *106*, 5527–5535.

(18) Hou, T. J.; Zhu, L. L.; Chen, L. R.; Xu, X. J. Mapping the binding site of a large set of quinazoline type EGF-R inhibitors using molecular field analyses and molecular docking studies. *J. Chem. Inf. Comput. Sci.* **2003**, *43*, 273–287.

(19) Lepsik, M.; Kriz, Z.; Havlas, Z. Efficiency of a second-generation HIV-1 protease inhibitor studied by molecular dynamics and absolute binding free energy calculations. *Proteins* **2004**, *57*, 279–293.

(20) Hou, T. J.; Yu, R. Molecular dynamics and free energy studies on the wild-type and double mutant HIV-1 protease complexed with amprenavir and two amprenavir-related inhibitors: Mechanism for binding and drug resistance. *J. Med. Chem.* **2007**, *50*, 1177–1188.

(21) Lee, M. R.; Duan, Y.; Kollman, P. A. Use of MM-PB/SA in estimating the free energies of proteins: Application to native, intermediates, and unfolded villin headpiece. *Proteins* **2000**, *39*, 309–316.

(22) Hou, T. J.; Chen, K.; McLaughlin, W. A.; Lu, B. Z.; Wang, W. Computational analysis and prediction of the binding motif and protein interacting partners of the Abl SH3 domain. *Plos. Comput. Biol.* **2006**, *2*, 46–55.

(23) Wang, W.; Kollman, P. A. Computational study of protein specificity: The molecular basis of HIV-1 protease drug resistance. *Proc. Natl. Acad. Sci. U.S.A.* **2001**, *98*, 14937–14942.

(24) Wang, J. M.; Hou, T. J.; Xu, X. J. Recent advances in free energy calculations with a combination of molecular mechanics and continuum models. *Curr. Comput.-Aided Drug Des.* **2006**, *2*, 287–306.

(25) Kollman, P. A.; Massova, I.; Reyes, C.; Kuhn, B.; Huo, S. H.; Chong, L.; Lee, M.; Lee, T.; Duan, Y.; Wang, W.; Donini, O.; Cieplak, P.; Srinivasan, J.; Case, D. A.; Cheatham, T. E. Calculating structures and free energies of complex molecules: Combining molecular mechanics and continuum models. *Acc. Chem. Res.* **2000**, *33*, 889–897.

(26) Iversen, L. F.; Moller, K. B.; Pedersen, A. K.; Peters, G. H.; Petersen, A. S.; Andersen, H. S.; Branner, S.; Mortensen, S. B.; Moller, N. P. H. Structure determination of T cell protein-tyrosine phosphatase. *J. Biol. Chem.* **2002**, *277*, 19982–19990.

(27) Berman, H. M.; Westbrook, J.; Feng, Z.; Gilliland, G.; Bhat, T. N.; Weissig,;Shindyalov, I. N.; Bourne, P. E. The Protein Data Bank. *Nucleic Acids. Res.* **2000**, *28*, 235–242.

(28) Barford, D.; Flint, A. J.; Tonks, N. K. Crystal-Structure of Human Protein-Tyrosine-Phosphatase 1b. *Science* **1994**, *263*, 1397–1404.

(29) *SYBYL 7.1*; Tripos International, 1699 South Hanley Rd., St. Louis, MO 63144, U.S.A.

(30) Case, D. A.; Cheatham, T. E.; Darden, T.; Gohlke, H.; Luo, R.; Merz, K. M.; Onufriev, A.; Simmerling, C.; Wang, B.; Woods, R. J. The Amber biomolecular simulation programs. *J. Comput. Chem.* **2005**, *26*, 1668–1688.

(31) Jorgensen, W. L.; Chandrasekhar, J.; Madura, J. D.; Impey, R. W.; Klein, M. L. Comparison of Simple Potential Functions for Simulating Liquid Water. *J. Chem. Phys.* **1983**, *79*, 926–935.

(32) *Gaussian 03, Revision C.02*; Frisch, M. J.; Trucks, G. W.; Schlegel, H. B.; Scuseria, G. E.; Robb, M. A.; Cheeseman, J. R.; Montgomery, J. A., Jr.; Vreven, T.; Kudin, K. N.; Burant, J. C.; Millam, J. M.; Iyengar, S. S.; Tomasi, J.; Barone, V.; Mennucci, B.; Cossi, M.; Scalmani, G.; Rega, N.; Petersson, G. A.; Nakatsuji, H.; Hada, M.; Ehara, M.; Toyota, K.; Fukuda, R.; Hasegawa, J.; Ishida, M.; Nakajima, T.; Honda, Y.; Kitao, O.; Nakai, H.; Klene, M.; Li, X.; Knox, J. E.; Hratchian, H. P.; Cross, J. B.; Bakken, V.; Adamo, C.; Jaramillo, J.; Gomperts, R.; Stratmann, R. E.; Yazyev, O.; Austin, A. J.; Cammi, R.; Pomelli, C.; Ochterski, J. W.; Ayala, P. Y.; Morokuma, K.; Voth, G. A.; Salvador, P.; Dannenberg, J. J.; Zakrzewski, V. G.; Dapprich, S.; Daniels, A. D.; Strain, M. C.; Farkas, O.; Malick, D. K.; Rabuck,A. D.; Raghavachari, K.; Foresman, J. B.; Ortiz, J. V.; Cui, Q.; Baboul, A. G.; Clifford, S.; Cioslowski, J.; Stefanov, B. B.; Liu, G.; Liashenko, A.; Piskorz, P.; Komaromi, I.; Martin, R. L.; Fox, D. J.; Keith, T.; Al-Laham, M. A.; Peng, C. Y.; Nanayakkara, A.; Challacombe, M.; Gill, P. M. W.; Johnson, B.; Chen, W.; Wong,M. W.; Gonzalez, C.; Pople, J. A. Gaussian, Inc.: Wallingford, CT, 2004.

(33) Bayly, C. I.; Cieplak, P.; Cornell, W. D.; Kollman, P. A. A Well-Behaved Electrostatic Potential Based Method Using Charge Restraints for Deriving Atomic Charges - the Resp Model. *J. Phys. Chem-Us.* **1993**, *97*, 10269–10280.

(34) Duan, Y.; Wu, C.; Chowdhury, S.; Lee, M. C.; Xiong, G. M.; Zhang, W.; Yang, R.; Cieplak, P.; Luo, R.; Lee, T.; Caldwell, J.; Wang, J. M.; Kollman, P. A point-charge force field for molecular mechanics simulations of proteins based on condensed-phase quantum mechanical calculations. *J. Comput. Chem.* **2003**, *24*, 1999–2012.

(35) Wang, J. M.; Wolf, R. M.; Caldwell, J. W.; Kollman, P. A.; Case, D. A. Development and testing of a general amber force field. *J. Comput. Chem.* **2004**, *25*, 1157–1174.

(36) Darden, T.; York, D.; Pedersen, L. Particle Mesh Ewald -and.Log(N) Method for Ewald Sums in Large Systems. *J. Chem. Phys.* **1993**, *98*, 10089–10092.

(37) Ryckaert, J. P.; Ciccotti, G.; Berendsen, H. J. C. Numerical-Integration of Cartesian Equations of Motion of a System with Constraints -

Molecular-Dynamics of N-Alkanes. *J. Comput. Phys.* **1977**, *23*, 327–341.

(38) Gilson, M. K.; Sharp, K. A.; Honig, B. H. Calculating the Electrostatic Potential of Molecules in Solution - Method and Error Assessment. *J. Comput. Chem.* **1988**, *9*, 327–335.

(39) Gohlke, H.; Kiel, C.; Case, D. A. Insights into protein-protein binding by binding free energy calculation and free energy decomposition for the Ras-Raf and Ras-RaIGDS complexes. *J. Mol. Biol.* **2003**, *330*, 891–913.

(40) Hou, T. J.; McLaughlin, W.; Lu, B.; Chen, K.; Wang, W. Prediction of binding affinities between the human amphiphysin-1 SH3 domain and its peptide ligands using homology modeling, molecular dynamics and molecular field analysis. *J. Proteome Res.* **2006**, *5*, 32–43.

(41) Hou, T. J.; Zhang, W.; Case, D. A.; Wang, W. Characterization of domain-peptide interaction interface: A case study on the amphiphysis-1 SH3 domain. *J. Mol. Biol.* **2008**, *376*, 1201–1214.

CI800104S